

## RADIO PULSE SHAPES, FLUX DENSITIES, AND DISPERSION OF PULSAR NP 0532

J. M. RANKIN

Department of Physics and Astronomy, University of Iowa, Iowa City

J. M. COMELLA, H. D. CRAFT, JR., D. W. RICHARDS, AND D. B. CAMPBELL  
 Cornell-Sydney University Astronomy Center, Arecibo Observatory, Arecibo, Puerto Rico

AND

C. C. COUNSELMAN III

Department of Earth and Planetary Sciences, Massachusetts Institute of Technology

Received 1970 March 9; revised 1970 July 27

### ABSTRACT

Observations of NP 0532 at frequencies between 65 and 611 MHz are reported. At high frequencies the main pulse is found to be double; the second component and the interpulse are of very short duration ( $< 300 \mu\text{sec}$ ) at 430 MHz. At lower frequencies the pulses become progressively broader until, below about 120 MHz, only one broad pulse is observed. Measurements of the pulsed flux density yield a spectral index of  $-2.9 \pm 0.4$  above 150 MHz, but a sharp turnover in the spectrum occurs at about 100 MHz. The law of pulse delay as a function of frequency agrees closely with the tenuous-plasma dispersion relation, and an improved value of the dispersion measure is given.

The variation with radiofrequency of the pulse shape and the low-frequency turnover of the pulsed flux density are explained as effects of scattering in the ionized interstellar medium, if one assumes frequency-independent pulse shape and constant spectral index of the source itself. The compact source observed at low frequencies in the Crab Nebula may be the pulsar.

### I. INTRODUCTION

The discovery of dispersed pulse signals from the Crab Nebula was reported by Staelin and Reifenstein (1968) more than two years ago. The period and other properties of the new pulsar, NP 0532, were then measured by Comella *et al.* (1969), who used the 1000-foot reflector at the Arecibo Observatory. Richards and Comella (1969) measured the slowdown rate of NP 0532; and optical emissions, first reported by Cocke, Disney, and Taylor (1969), were confirmed by several other groups (Lynds, Maran, and Trumbo 1969; Nather, Warner, and MacFarlane 1969; Miller and Wampler 1969; Duthie *et al.* 1969). Detection of the pulsar has now been reported at hard X-ray (Fishman, Harnden, and Haymes 1969), soft X-ray (Boldt *et al.* 1969; Fritz *et al.* 1969), and infrared wavelengths (Neugebauer *et al.* 1969). Thus, a large body of complementary information has come into the literature relative to the pulsar in the Crab Nebula. The object is unique in its amenability to study over such a wide interval of wavelengths and in its association with a recent and well-known supernova remnant.

At Arecibo the pulsar has been regularly observed since soon after its discovery in 1968. Some of the work has been reported previously (Comella *et al.* 1969; Richards and Comella 1969). However, some recent efforts, together with general improvements in experimental design, have greatly increased the precision of radiofrequency observations of NP 0532. We thus wish in this paper to report some new results which have not heretofore been published as well as to try to systematize better some of the phenomena occurring in the radiofrequency portion of the pulsar's spectrum.

Some of the material in this paper has been reported (Richards 1969; Rankin *et al.* 1969).

## II. OBSERVATIONAL TECHNIQUE

Observations of the pulsar in the Crab Nebula are complicated by very strong radiation from the nebula itself. Averages containing a minimum of  $10^4$  pulses (about 5 minutes) are required merely to detect the pulsar against the continuum background. The pulsar does emit single pulses of very large amplitude which are detectable above the nebular continuum (Staelin and Reifenstein 1968; Staelin and Sutton 1969; Goldstein and Meisel 1969; Heiles, Campbell, and Rankin 1970); however, they are sufficiently rare (about one pulse in  $10^4$ ) that, for purposes of measuring most properties of the pulsar, they are not very useful.

The short period and narrow pulse structure of NP 0532 require much higher data rates than other pulsars. Data have been taken both asynchronously and, once the period of the pulsar was sufficiently well established, synchronously with the pulsar. The latter

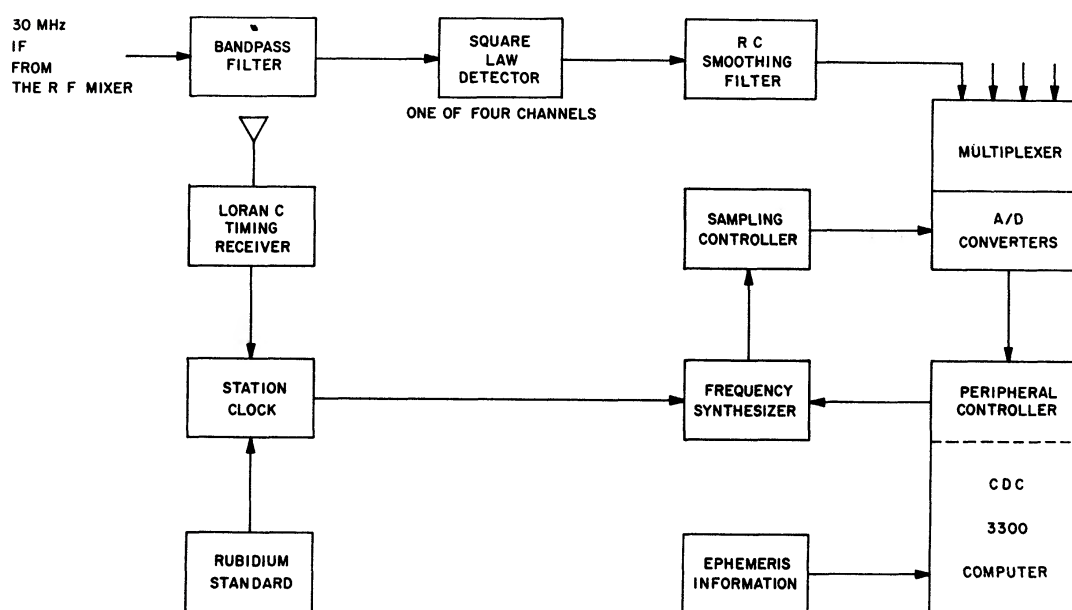


FIG. 1.—Block diagram of the computer-controlled synchronous-sampling equipment

technique is more efficient, for it allows averaging to be done while the data are being taken. Synchronous sampling is almost universally employed in optical observations of the pulsar by use of multiscalers; in the present case, however, the averaging was done with an on-line digital computer after digitizing the radio signal.

Figure 1 is a block diagram of the synchronous sampling equipment. A computer-controlled frequency synthesizer and a preset counter in the sampling controller are used to produce a time base which has the apparent period of the pulsar. In calculating the synthesizer frequency, the computer program allows for both known changes in the intrinsic period and effects of the Earth's motion. Accumulated phase error amounts to less than a few tens of  $\mu\text{sec}$  in a 3-hour period. Word length on the computer limits runs to about 15 minutes each, and a new apparent period is computed at the beginning of each run and passed to the frequency synthesizer. During each pulsar period, 1024 samples are taken at intervals of  $32 \mu\text{sec}$  on each of four-channels. There is an unsampled interval of about  $380 \mu\text{sec}$ .

## III. OBSERVATIONAL RESULTS

## a) Pulse Shapes: Observations

Preliminary average pulse shapes have been published previously for NP 0532 for radiofrequencies down to about 200 MHz (Comella *et al.* 1969) and also for optical frequency (Lynds *et al.* 1969; Warner, Nather, and MacFarlane 1969; Wampler, Scargle, and Miller 1969). All show the same general structure, that is, a single main pulse followed about 14 msec later by an interpulse of somewhat smaller intensity. The time resolution of the published radiofrequency average pulse shapes has been of the order of 1 msec or more, while that of the optical pulses was about 10  $\mu$ sec.

Radiofrequency measurements have now been performed with substantially better time resolution and over a wider range of frequencies. Figure 2 shows the average pulse shapes measured at frequencies from 430 MHz down to 73.8 MHz, and Table 1 gives the receiver parameters pertinent to these observations. The relative phases are arbitrary; no phase relationships are implied by the manner of the presentation. Although in each case the pulse shape shown is an average over  $10^5$  or more pulses as described above, smearing due to errors in the assumed period is less than about 40  $\mu$ sec. The effective

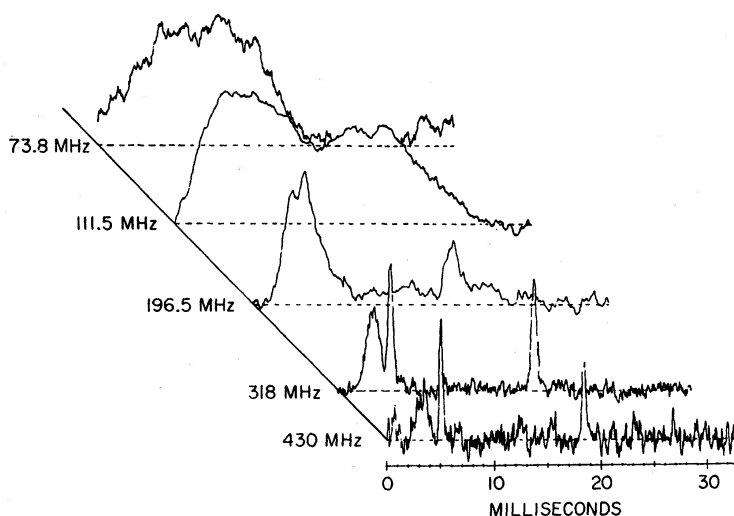


FIG. 2.—Observed average pulse shapes at 430, 318, 196.5, 111.5, and 73.8 MHz. Phases of pulses are arbitrary.

TABLE 1

RADIOMETER DATA RELEVANT TO PULSE-SHAPE DETERMINATION

Frequency (MHz)	Date of Observation (1969)	Length of Observation ( $10^6$ Periods)	Intermediate-Frequency Bandwidth (kHz)	Post-Detection Time Constant (msec)	Sweep Rate (kHz msec $^{-1}$ )	$\tau_{opt}$ ( $\mu$ sec)	$\tau_{real}$ ( $\mu$ sec)
430.....	July 30	1.92	25	0.10	168	110	250
318.....	August 22	1.43	25	0.10	67.7	170	420
196.5.....	July 12	1.92	5	0.20	16.0	350	550
111.5.....	August 10	2.38	5	1.00	2.9	830	2600
73.8.....	August 10	2.38	8	3.30	0.85	1500	11500

limit on time resolution is set by the pre-detection filter passband and the post-detection filter time constant. The bandwidths and time constants were chosen to give the best possible time resolution consistent with an acceptable signal-to-noise ratio (S/N). Further improvement in resolution requires a technique for reducing the dispersion before detection (Staelin and Sutton 1969).

It is clear from Figure 2 that for NP 0532 (more than for any other known pulsar), the pulse shape is a strong function of radiofrequency. (Weak dependence of pulse width on frequency, as  $f^{-1/4}$ , has been observed in CP 1133 by Craft and Comella [1968] and in NP 0527 by Zeissig and Richards [1969].) At the higher frequencies in the diagram, the main pulse is resolved into two components, the latter of which is quite narrow and will be referred to as the main pulse. The earlier component, which is generally of smaller amplitude and much greater width, will be called the precursor to the main pulse. The main pulse is followed less than half a period later by an interpulse of similarly narrow half-width. In the average of many tens of thousands of pulses at 430 MHz, the widths (full width at half-maximum) of the main pulse and of the interpulse are about 300 and 400  $\mu\text{sec}$ , respectively, and the ratio of their amplitudes is approximately 1.4.

The morphology of the 318-MHz pulse differs from that at 430 MHz only in that the widths at half-maximum of the main pulse and interpulse are approximately twice as great. At 196.5 MHz, the precursor merges with the main pulse to yield a single broad main pulse which typically shows two distinct peaks which do not seem to be further resolvable. The interpulse is still distinct but is connected to the main pulse by a slight rise in the baseline which will be discussed below. At 111.5 MHz the interpulse and main pulse overlap to yield a broad single pulse which occupies the greater part of the pulse period. The onset ramp is still quite steep (rise time about 3 msec), and the interpulse is visible as a small feature some 14 msec after the onset ramp. At 102 MHz and below, the pulse is still broader. No features corresponding to those at higher frequencies can be identified; all that can definitely be said is that there is power in the fundamental 30.212-Hz Fourier component.

The intervals between the various components of the pulse can be measured relatively accurately at high frequency. The precursor precedes the main pulse by  $1.64 \pm 0.1$  msec. This error is rather large owing to the large width and small amplitude of the precursor. The interval between the bisector of the main pulse and that of the interpulse is  $13.37 \pm 0.03$  msec. These errors are the standard deviations of several measurements. No variation either in time or with frequency has been observed in either of the above intervals.

In contrast to the two narrow components which are of fairly constant shape and amplitude, the precursor is time-variable on a scale of a few tens of minutes at 318 MHz. This is illustrated by Figure 3, which shows eleven consecutive, 6-minute observations in three channels separated by 1 MHz. The variations in the amplitude of the precursor relative to the main pulse are apparent. The precursor often contributes as much energy as the main pulse, or even more; then again, it occasionally disappears altogether. The relative amplitudes of the precursor show a general tendency to be correlated in the three channels; however (if comparison is restricted to the two identical 25-kHz channels), there seem to be several cases where a significant decorrelation occurs over an interval of only 1 MHz. Investigation of the variability of the precursor at other frequencies is difficult since at lower frequencies a distinct precursor is not observed and at higher frequencies a sufficiently good S/N is not attained in a few minutes of observation.

It should be noted that these observations were made with linearly polarized antennas. Linear polarization in the precursor, as reported by Campbell, Heiles, and Rankin (1970), might explain the time variations in relative pulse intensity. Polarization could not, however, explain a frequency decorrelation in pulse amplitude over an interval of 1 MHz if the rotation measure to NP 0532 is similar to that for the Crab Nebula itself ( $-25 \text{ rad m}^{-2}$  [Gardner and Davies 1966]).

At high frequencies, the ratio of the total energy of the interpulse to that of the main

pulse may be determined from the areas under the respective pulses. At both 318 and 430 MHz, this ratio is  $80 \pm 5$  percent. The ratio of the energy of the precursor to that of the main pulse is more difficult to determine owing to the variability and smaller peak flux density of the precursor. Some measurements with large bandwidths at 318 MHz would indicate a ratio as large as 2 which is quite compatible with the observation of large linear polarization in the precursor. A long-term average (which averages over all states of linear polarization) yields a ratio of more like 1.2.

Finally, it is clear from the 196.5-MHz pulse in Figure 2 that not all emission is restricted to the three principal pulse components. Measurable emission occurs throughout the interval between the main pulse and the interpulse. Warner *et al.* (1969) have observed a similar rise in the baseline in the optical. Emission between the principal pulse

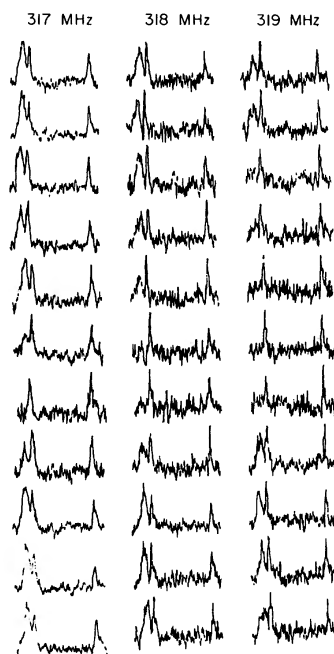


FIG. 3.—Consecutive 6-minute average pulse shapes at 317 MHz (bandwidth: 50 kHz; 0.1 msec), 318 MHz (25 kHz; 0.1 msec), and 319 MHz (25 kHz; 0.1 msec).

components becomes increasingly hard to observe at high radiofrequency as the S/N decreases. At low frequency, however, it may not be possible to account for the pulse shape without considering the rise in the baseline (see § IIIc below).

#### b) Flux Densities: Observations

Preliminary measurements of flux density have been given by Comella *et al.* (1969) for frequencies above 196.5 MHz. Measurements have now been extended to lower frequencies, and experimental precision has been substantially improved. Radiometer gain calibrations were made with a noise source which was pulsed at a known rate. Radiometer gain stability was continuously monitored by measuring the receiver total power which was dominated by the Crab Nebula continuum. Scans of 3C 123 and in special cases the Crab Nebula itself were used to provide absolute flux-density calibration. The assumed values of the flux densities of the reference sources given in Table 2 have been interpolated from measurements by Kellermann, Pauliny-Toth, and Williams (1969). The energy per pulse was obtained by integrating over the average pulse after subtracting

the baseline; the resulting energy is equal to the averaged pulse flux density multiplied by the pulse period.

The resulting measurements of flux density together with other data are given in Table 2. The error quoted at a particular frequency is the computed standard deviation of values obtained from several days' observations. Whenever possible, the data for a particular frequency and day were also reduced in several parts. The values obtained from these partial averages agree to within the quoted errors. Thus, variability on a scale of less than several months seems to have been effectively averaged. It is not clear from the data whether or not the large errors at some frequencies are due to instrumental variations, to intrinsic variability, or to polarization effects. Campbell *et al.* (1970) have observed intrinsic variability at 430 MHz.

These average flux-density measurements are plotted as circles in Figure 4 in units of flux units ( $1 \text{ flux unit} = 10^{-26} \text{ W m}^{-2} \text{ Hz}^{-1}$ ), and compact source data from Bridle's (1970) Table 2 appear as squares. Unpublished upper limits of the pulsar's flux at 2388 MHz and 15 GHz were generously given by Downs and Reichley (1970) and by one of us

TABLE 2  
NP 0532 SPECTRAL DATA

Frequency (MHz)	Assumed Flux Density, 3C 123 (f.u.)	Assumed Flux Density, Tau A (f.u.)	Bandwidth (kHz)	Number of Pulses ( $\times 10^6$ )	Pulsed Energy, NP 0532 ( $\times 10^{-26} \text{ J m}^{-2} \text{ Hz}^{-1}$ )	Average Pulsed Flux Density, NP 0532 (f.u.)	Predicted Flux Density (f.u.)
65.0.....	...	2071	1.0	0.68	<0.14	<4.2	3.1
73.8.....	357	...	1.0-2.1	0.71	0.16 $\pm$ 0.1	4.8 $\pm$ 3.0	5.6
89.6.....	...	1882	2.1	0.85	0.40 $\pm$ 0.2	12.1 $\pm$ 6.0	13.8
102.0.....	...	1810	5.0	0.33	0.50 $\pm$ 0.1	15.0 $\pm$ 3.0	22.1
111.5.....	265	...	2.1	0.93	0.66 $\pm$ 0.2	20.0 $\pm$ 6.0	25.1
196.5.....	177	...	5.0-25	0.66	0.21 $\pm$ 0.05	6.4 $\pm$ 1.5	6.6
430.0.....	105	...	50-125	1.15	0.027 $\pm$ 0.012	0.82 $\pm$ .35	0.64
611.0.....	82.9	...	125-500	0.95	0.0072 $\pm$ 0.002	0.22 $\pm$ .06	0.23
2388 *.....	...	...	...	...	<0.0004	<0.012	0.004
15000†.....	...	...	...	...	<0.0005	<0.015	1.8 $\times 10^{-5}$

\* Downs and Reichley (1970).

† Counselman (1970).

(C. C. C.), respectively. Two aspects of the spectrum are striking: the sharpness of the cutoff at about 100 MHz, and the steepness of the high-frequency spectral decline. As discussed in the following paragraph, the high-frequency spectral index is substantially larger than was previously thought (Comella *et al.* 1969).

The pulsar data for 196.5 MHz and above can be represented by the expression  $S = k(f/f_0)^a$ , where  $k = 0.80 \pm 0.13$ ,  $a = -2.9 \pm 0.4$ , and  $f_0 = 400 \text{ MHz}$ . The best fit and its corresponding error envelope are shown in Figure 4 as solid curves. The fitted curves were calculated via a nonlinear weighted, least-square error regression analysis (Whittaker and Robinson 1967). Application to the pulsar and compact source spectral data is considered in the Appendix. The shapes of the solid and short-dashed curves at low frequency depend upon the high-frequency fit and various assumptions relative to the pulse broadening which will be discussed below. The two long-dashed curves are extrapolations of the high-frequency error envelopes to lower frequencies.

### c) Pulse Broadening

In discussing the strong systematic broadening of the pulse displayed by the pulsar in the Crab Nebula at lower frequencies, it is first necessary to consider any broadening due

to the radiometer. Uncorrected for broadening in the receiver, the pulse width scales approximately as  $f^{-2.5}$  (Richards 1969). There are three causes of instrumental pulse broadening: (a) use of a finite bandwidth to observe a pulse swept by dispersion, (b) the rise time of the filter used to define the intermediate-frequency passband, and (c) the post-detection filter time constant. Let  $\tau_1$ ,  $\tau_2$ , and  $\tau_3$  represent the effective integration time of sources *a*, *b*, and *c*, respectively. Within factors of 2, their effects may be estimated as follows:

$$\tau_1 \approx \Delta f / |df/dt| ; \quad \tau_2 \approx 1/\Delta f ; \quad \tau_3 = 2\tau_0 , \quad (1)$$

where

$$|df/dt| = f^3/2D \quad (2)$$

and  $\Delta f$  is the width of the intermediate-frequency bandpass,  $\tau_0$  is the RC time constant of the post-detection filter, and  $D$  is the dispersion constant as defined below. Since the total broadening may be computed as the root mean square of the individual effects, optimum time resolution is obtained when  $\tau_1$  is equal to  $\tau_2$  and when  $\tau_3 \ll \tau_1, \tau_2$ . Thus, the bandwidth at a given observing frequency should approximate the square root of the sweep rate  $|df/dt|$ , and the best resolution obtainable,  $\tau_{\text{opt}}$ , is about  $|0.5 df/dt|^{-1/2}$ .

It was necessary, in general, to use a bandwidth somewhat larger than optimum in order to obtain adequate S/N in a reasonable observing time. Thus, estimates of both the actual,  $\tau_{\text{real}}$ , and optimum time resolutions appear in Table 1. It is clear from Figure 2 and Table 1 that the observed pulsewidths at 430 and 318 MHz are largely of instrumental origin; only at 196.5 MHz is the resolution close to the optimum value.

While the radiometer does affect the high-frequency pulse shapes, it is clearly not responsible for the dramatic pulse broadening at lower frequencies. We have, therefore, explored the possibility that the broadening could be the result of propagation effects and have compared the observations with a model in which the shape of the pulse when it leaves the pulsar is the same at all radiofrequencies, but is broadened in transit to the Earth by multipath propagation in the interstellar medium, the broadening being greater at lower frequencies.

If at high frequency the pulse width, and thus the shape, is predominantly the result of instrumental broadening, and if at low frequency the interstellar medium is principally responsible for the pulse shape, it then follows that at no frequency is the intrinsic pulse shape (the pulse shape emitted at the pulsar) observed directly. Guided by the 430- and 318-MHz observations where multipath broadening is presumably small, we have attempted to construct an intrinsic pulse. Broadening in the radiometer was modeled by convolution of the intrinsic pulse first with an intermediate-frequency filter-response function and then with an exponential ( $e^{-\tau/\tau_0}$ ,  $\tau \geq 0$ ) representing the post-detection filter. (The effect of the pre-detection filter rise time is negligibly small.)

The artificial pulse shapes resulting from the convolutions, or templates as they will be called, are directly comparable with the observed pulses. After some adjustment an acceptable intrinsic pulse, which is shown in Figure 5, *a*, was constructed from the data in § IIIa. The intervals between the various components conform to the data given above. Relative to the main pulse, the total energies of the precursor and the interpulse are 1.2 and 0.8, respectively. A total relative energy of 0.9 has also been distributed along the baseline as discussed previously. This last contribution is too small to be well illustrated on the figure; it must, however, be included to account for both the rise in the baseline observed at 196.5 MHz and the shape of the region between the main pulse and interpulse at 111.5 MHz.

The assumption that the intrinsic pulse is independent of frequency is somewhat further justified as follows: It has only been required that the intrinsic pulse yield reasonable high-frequency templates when corrected for radiometer broadening. The above requirement is not a strenuous constraint as the intrinsic pulse is always convolved with a relatively broad function and thus it is necessary only to space the components of the

pulse properly and endow them with an appropriate quantity of energy. Down to 196.5 and with somewhat less certainty to 111.5 MHz, neither the spacing nor the relative energies of the pulse components are observed to change significantly. It is then not unreasonable to assume that no strong change in the intrinsic shape of the pulse occurs over the entire range of frequencies from 430 to 65 MHz.

The effects of the medium are described by a frequency-dependent probability-density function of excess travel time,  $p(f, \Delta t)$ . The frequency dependence of the width of the

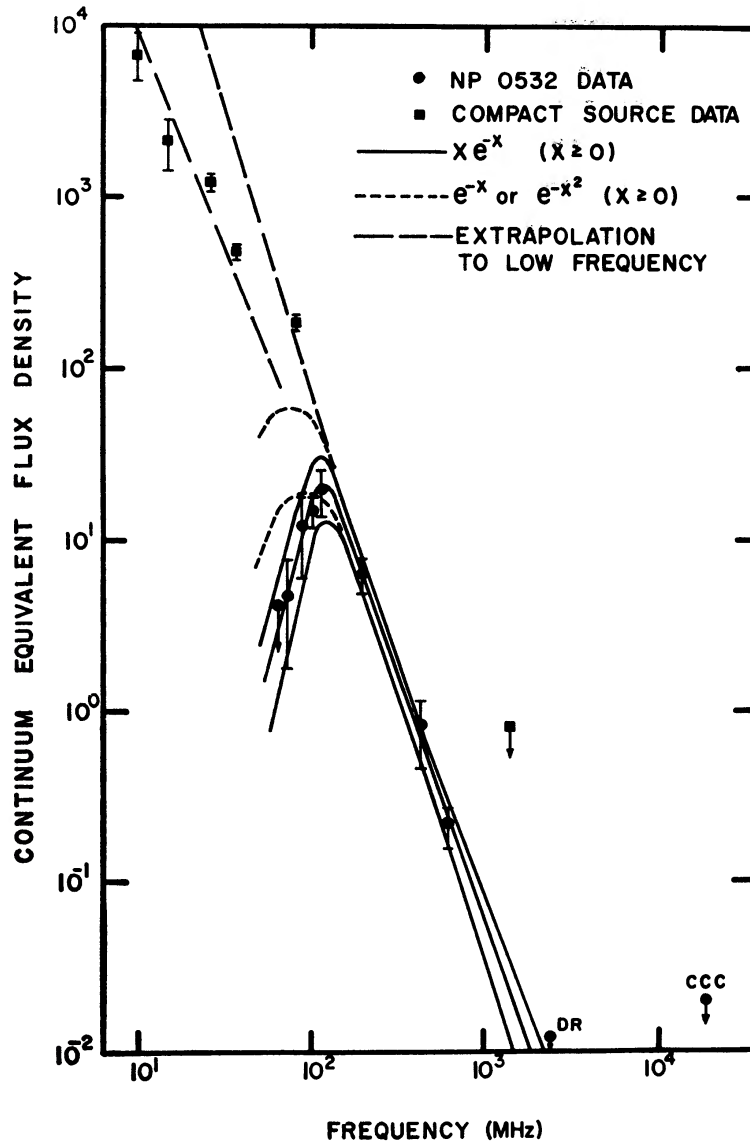


FIG. 4.—Radiofrequency spectra of pulsar NP 0532 and the compact source in the Crab Nebula. *Solid curve*, fit to the pulsar's spectrum by using the  $xe^{-x}$  broadening function; the parallel curves denote the associated error envelope. Short dashed curves give the error envelope of a similar fit if the exponential or half-Gaussian density functions are assumed; long dashed lines denote the range of possible extrapolations of the pulsar's high-frequency spectrum. Compact-source flux-density measurements are from Bridle (1970). Upper limits on the pulsar's flux density are by Downs and Reichley (1970) and by one of us (C. C. C.)

density function we take to be given by a power law. The pulse-width parameter  $W$  is defined by

$$W = A(f_0/f)^\delta, \quad (3)$$

where  $A$  and  $\delta$  are to be determined; and, in terms of  $W$ , the probability-density function may be written as a function of one variable:

$$p(f, \Delta t) = W^{-1}p'(\Delta t/W). \quad (4)$$

An important quantity to determine is the spectral index  $\delta$ , as it may be compared with certain theoretical predictions. Most of the information relative to determining  $\delta$  is contained in the lower-frequency pulse shapes since at high frequency the pulse width is largely of instrumental origin. It is first necessary to find the form of the density function  $p'(\Delta t/W)$ , although, as will be shown, the particular form of  $p'(\Delta t/W)$  does not strongly affect the determination of  $\delta$ .

Several arbitrarily chosen probability-density functions have been tried in order to reproduce the observed pulse profiles. In each attempt, the intrinsic pulse was convolved with the probability-density function and with the functions representing the effects of the radiometer. The final template resulting from the three cascaded convolutions was then compared with the observed pulse shapes.

The constant  $A$  in equation (3) was adjusted to match the pulse width observed at 196.5 MHz ( $f_0$  in eq. [3] is 196.5 MHz). Template pulses for frequencies other than 196.5 MHz were computed similarly except that the width of the probability-density function was adjusted according to equation (3). For a given density function, a two-parameter family of template pulses was generated which corresponded to the frequency of observation on the one hand and the value of  $\delta$  in equation (3) on the other. Comparison of the templates with the observed average pulse shapes then determined  $\delta$ .

A Gaussian probability-density function was used in the first attempt to reproduce the observed pulse shapes. Only values of  $\delta$  near 4 gave pulse shapes resembling those observed; however, the resulting template shapes were not very satisfying. The problem with the Gaussian is clearly its symmetry; a highly asymmetrical function is required to account for the onset ramp of the 111.5-MHz pulse.

Given the defects of the Gaussian, a truncated exponential ( $e^{-\Delta t/W}$ ,  $0 \leq \Delta t \leq \infty$ ) was next investigated. Template pulses calculated by using the exponential density function and with a value for  $\delta$  equal to 4 are given in Figure 5, *b*. These pulses qualitatively resemble the observed pulses for  $\delta$  in the range 2.5–5.5. However, more detailed comparison of the pulse widths of the templates with those of the observed pulses again restricts the acceptable range of  $\delta$  to values near 4. At high frequency, the shapes of the template pulses agree quite well with those in Figure 2, but at 111.5 MHz the shape of the template pulse is more sharply peaked than is the observed shape.

Another attempt to reproduce the observed pulse profiles was made by using the function  $\exp(-\Delta t^2/2W^2)$ , ( $0 \leq \Delta t \leq \infty$ ); that is, half a Gaussian. For frequencies of 196.5 MHz and higher, the templates are very similar to the exponential templates but the 111.5-MHz template is substantially improved.

The results obtained with the Gaussian, truncated exponential, and half-Gaussian functions point to the following conclusions regarding the actual probability-density function: (1) the function should be asymmetrical; (2) it should have a considerable "tail," comparable to, but perhaps not so long as, an exponential; and (3) the function should have a relatively steep rise in order to account for the observed 111.5-MHz onset ramp. For physical reasons, however, the discontinuity at zero delay of our truncated exponential and Gaussian functions seems objectionable. Only if all scattering in the interstellar medium took place in a single very thin screen would this discontinuity be possible. In fact, scattering probably occurs over some significant portion of the path

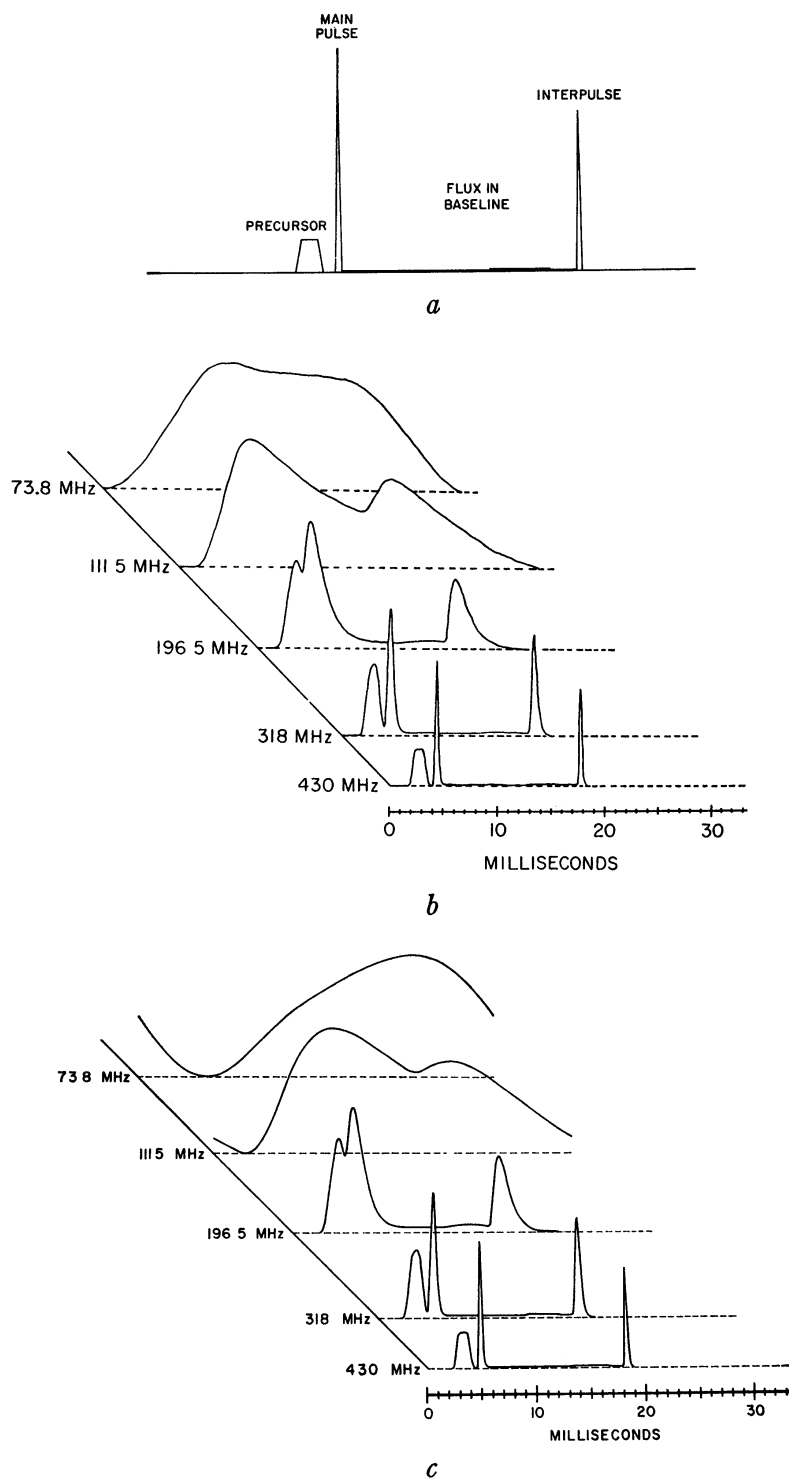


FIG. 5.—(a) Intrinsic pulse shape assumed in the broadening model. In (b) and (c) the intrinsic pulse is convolved with an exponential and an  $xe^{-x}$  probability-density function, respectively, representing multi-path propagation effects in the interstellar medium. (b) and (c) are also convolved with functions representing the pulse-broadening effects of the radiometer, and are thus directly comparable with the observed pulses in Fig. 2.

between the pulsar and the Earth, so that the initial value of the probability-density function must be small if not zero. Further, a positive initial slope seems to be required to explain the rapid cutoff of pulsed flux at low frequencies, as discussed below.

The above considerations led to the investigation of a number of other simple functions, two of which are worthy of mention. The Rayleigh density function,  $xe^{-x^2}$  ( $x \geq 0$ ), where  $x = \Delta t/W$ , yields 196.5-MHz pulse shapes with insufficiently long tails and 111.5-MHz shapes which are reminiscent of those resulting from the Gaussian; that is, the pulse shapes are excessively symmetrical.

Of the functions investigated, the one which comes closest to reproducing the pulse shapes (and the spectral cutoff described below) is the function  $xe^{-x}$  ( $x \geq 0$ ), where  $x = 2^{1/2} \Delta t/W$ . Templates for  $\delta$  equal to 4 corresponding to the pulse shapes in Figure 2 are illustrated in Figure 5, *c*. For frequencies 196.5 MHz and higher, the templates are very similar to the exponential templates; the 111.5-MHz template, however, is substantially improved. As the present probability-density function yields template pulses corresponding more closely to those observed than the other functions investigated, values of  $\delta$  deduced from these templates may be more significant than those deduced from the other functions.

Figure 6 is a plot of main pulse width versus frequency. The pulse widths of the  $xe^{-x}$  template pulses for various values of  $\delta$  are denoted by the symbols. The "error bars" denote the range of pulse widths exhibited by observed pulses. Finally, the solid curve is the locus of the width parameter,  $W$ , which has been normalized to the pulse width at 196.5 MHz and thus has the form  $0.85 (196.5/f)^4$  msec.

The pulse widths of the  $xe^{-x}$  template pulses are compatible with the observed pulse shapes for values of  $\delta$  between about 3.5 and 4.5. However, some systematic differences still exist between the template pulses and the observed pulses. The shape of the region between the main pulse and the interpulse is important in estimating the width of the main pulse (the quantity plotted in Fig. 6) and thus in determining approximate values of  $\delta$ . Thus, the index  $\delta$  cannot be determined to arbitrary precision from the data; however, the range quoted includes all such ambiguities. Particularly, our present determination of  $\delta$  cannot resolve the question, first raised by Huguenin and Taylor (1969), as to whether  $\delta$  does, indeed, for interstellar scintillations, take a value somewhat less than 4 (see also Lang 1969). Salpeter (1969) contends on theoretical grounds that  $\delta$  should assume values  $\gtrsim 4$ .

While the  $xe^{-x}$  density function reproduces both the observed pulse shapes and spectrum (discussed immediately below) reasonably well, there is little reason to attempt to justify it theoretically; it is simply the most satisfactory of a number of simple functions which were tried fortuitously. We only wish to argue the plausibility that interstellar scattering is responsible for the pulse broadening and that the broadening results in the pronounced loss of pulsating flux observed at low frequency. However, the proper broadening function is an important issue in the final resolution of both these questions, and thus a much more complicated attempt to determine the form of the interstellar broadening function is in progress. It is clear, however, that, given the assumptions of the above arguments, the simple exponential broadening function cannot adequately model the observed interstellar scattering.

The apparent turnover in the pulsar's spectrum at low frequency is now explained in terms of pulse broadening if it is assumed that the spectral index and intrinsic pulse shape of the pulsar are independent of frequency to somewhat below 100 MHz. It is clear from Figure 2 that at lower frequencies, as the pulse width approaches and exceeds the pulse period, the pulse shape will approach an average continuum value. For a particular frequency, probability-density function, and choice of  $A$  and  $\delta$  in equation (3), the fraction of the pulsar's flux which is still time-variable can be calculated. Only the variable component of the pulsar's flux density is measured; any continuum component cannot be distinguished from the large continuum background. The results of such a

calculation for  $\delta = 4$  in equation (3) and for both the half-Gaussian, exponential, and  $xe^{-x}$  density functions are given in Figure 4. The solid line is the spectrum which results from the last function; the dotted line, the others. The spectra are identical for frequencies above about 150 MHz; however, at low frequency a much better fit to the measured flux density is obtained with the function  $xe^{-x}$ . The spectra obtained are not strongly dependent upon values of  $A$  and  $\delta$  which are within the acceptable range of values (as discussed above), so that it does not seem possible to bring the spectrum deduced from the exponential templates into agreement with the observations. This con-

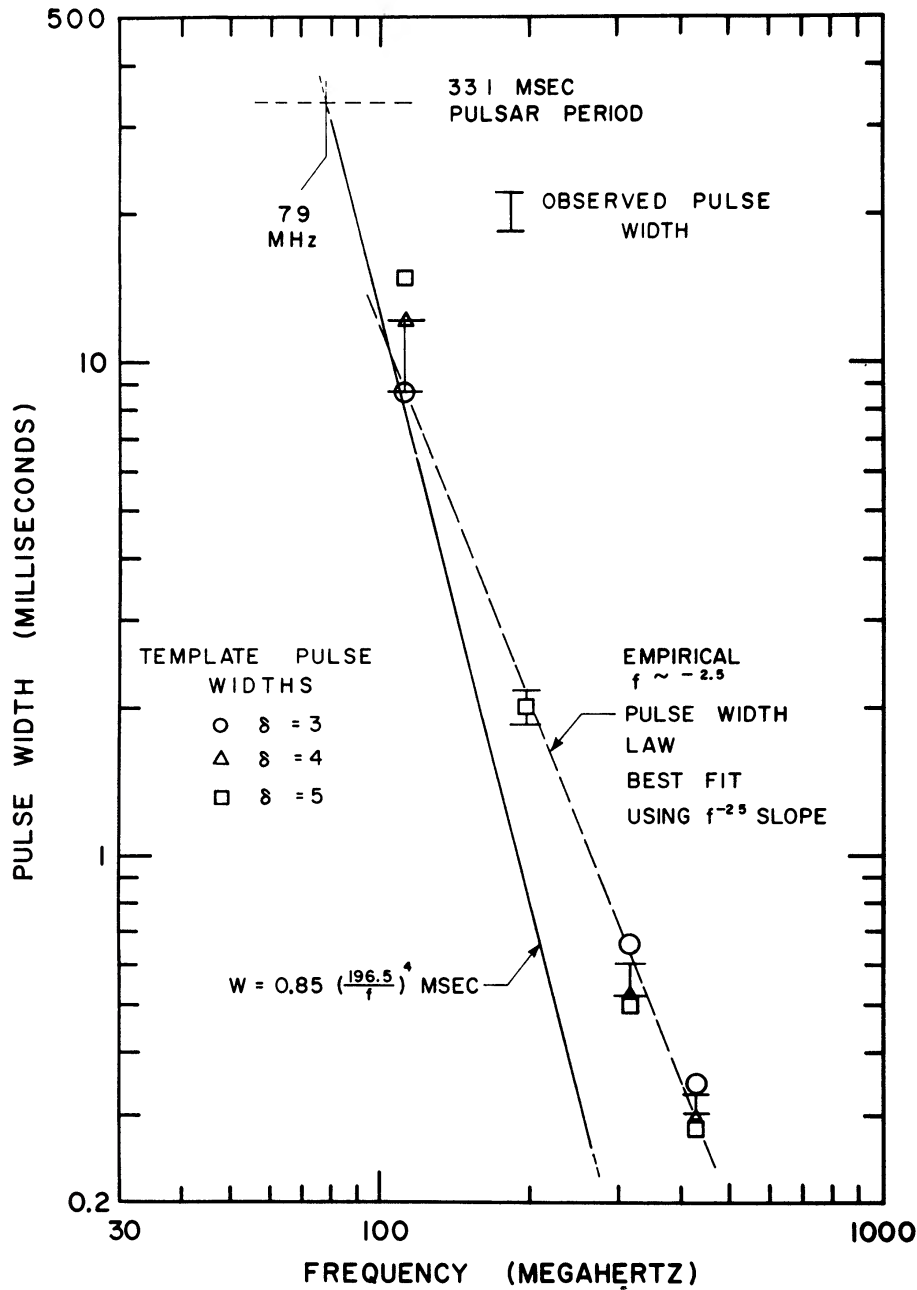


FIG. 6.—Frequency dependence of the observed width of the main pulse and those predicted by the broadening model using the  $xe^{-x}$  density function, where  $x = 2^{1/2} \Delta t/W$  and  $W = 0.85 (196.5/f)^{\delta}$ .

sideration argues against density functions which resemble the exponential or half-Gaussian, that is, functions which are monotonically decreasing.

Finally, it should be noted that the fluxes measured at low frequencies are dependent upon the receiver bandwidths and integration times. System parameters which result in optimum time resolution (as discussed above) also result in a maximum of observed flux variation. The observed spectrum given in Figure 4 is thus slightly dependent upon radiometer parameters, as are the derived fluxes which have been adjusted to include the same instrumental effects as the experimental spectrum. For reasonable system parameters, as in the present case, the flux lost by smoothing is small.

#### d) Dispersion Measure

Preliminary measurements of the integrated electron content between the Earth and NP 0532 have been described earlier (Comella *et al.* 1969). Measurements at that time showed that the delay between radio frequencies  $f_1$  and  $f_2$  followed the first-order plasma dispersion relation,

$$t_1 - t_2 = D(1/f_1^2 - 1/f_2^2), \quad (5)$$

to within the accuracy of measurement. The dispersion constant  $D$  in equation (5) is related to the integrated electron density as follows:

$$D = \frac{e^2}{8\pi^2 c \epsilon_0 m} \int_0^L N_e(s) ds, \quad (6)$$

where  $c$  is the velocity of light in a vacuum,  $m$  and  $e$  are the reduced electron mass and electron charge, and  $\epsilon_0$  is the permittivity of free space.  $N_e$  is the electron volume density

TABLE 3  
DISPERSION CONSTANTS, NP 0532

Delay 430 0-111.5 MHz (1969 May 31) = $17^{\circ}6835 \pm 0^{\circ}0004^*$
$D = 235700 \pm 70^{\dagger}$ sec-MHz <sup>2</sup>
$\int N_e ds = 17\ 5211 (\pm 0\ 0006) \times 10^{19} \ddagger e^- \text{ cm}^{-2}$
$= 56\ 78 \pm 0.02 \ddagger e^- \text{ pc cm}^{-3}$

\* Errors are standard errors

† See text for a discussion of the errors

‡ Physical constants from Allen (1964)

in the plasma, and  $L$  is the path length between the Earth and the pulsar. Subsequent measurements have improved upon the accuracy of the dispersion calculation through more accurate timing measurements at each radiofrequency and through the use of lower radiofrequencies than those used before.

Measurements of the sweep rate ( $-df/dt$ ) at radio frequencies of 430, 318, 196.5, 111.5, and 73.8 MHz showed that the sweep rate is proportional to the cube of the frequency over this range. This determination was not of high precision but was sufficient to effect an unambiguous identification of pulses received at the various frequencies involved. Final determination of the dispersion measure (DM), i.e., integrated electron density, for NP 0532 was then made from the measured total delay between 430 and 111.5 MHz, the data at 73.8 being such that the accuracy could not have been substantially improved through the use of that lower frequency. Table 3 gives the measured value for the dispersion constant and the deduced value for the integrated electron content. Both values have been referred to the solar-system barycenter as described below.

When the data determine  $D$  to an accuracy of about 0.1 percent, three additional

considerations need be included. The conversion of  $D$  to DM involves the use of physical constants whose values are not known to high precision. Also, since the orbital velocity of the Earth about the Sun modifies the apparent value of  $D$ , the value is referred to the solar-system barycenter. If  $D$  is the value for the constant in equation (5), as measured in a frame moving at velocity  $v$  away from the pulsar with respect to the barycenter, and  $D_0$  is the corresponding value in a frame stationary with respect to the barycenter, then to first order in  $\beta$  the two are related by

$$D = D_0(1 - \beta), \quad (7)$$

where  $\beta = v/c$ . Finally, consideration must be given to the presence of ions as well as electrons in the interstellar medium; as these are predominantly protons, it is sufficient simply to substitute the reduced electron mass as in equation (6).

The measurement of the delay between pulses at widely different radiofrequencies is complicated by the strongly frequency-dependent pulse morphology exhibited by NP 0532. In particular, it is not obvious which points on the 430- and 111.5-MHz pulses correspond. The values in Table 3 were derived by using, as a reference, the half-power

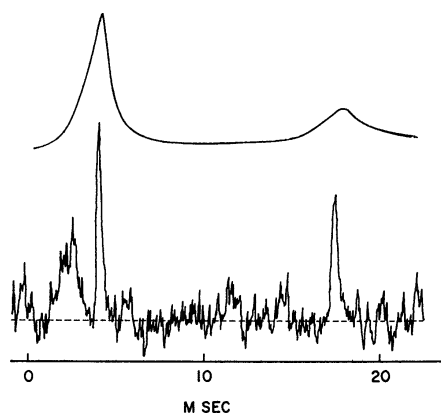


FIG. 7.—Comparison of the optical (*upper curve*, after Warner *et al.* 1969) and high-frequency radio pulse shapes. Alignment in time is arbitrary.

point of the leading edge of each pulse (the leading edge of the precursor at high frequency). This arbitrary choice of reference points is merely convenient, but it must be expected that there is present some contribution to the measured delay at 111.5 MHz due to the asymmetry of the multipath scattering probability density function. Since the width of this function is about 10 msec at 111.5 MHz, the uncertainty in the value of the dispersion constant quoted in Table 3 is derived from an assumed uncertainty of 5 msec in the 111.5-MHz delay, rather than from the much smaller observed scatter of these measurements. An improved value of the dispersion constant is expected to come from a simultaneous solution for dispersion and certain scattering parameters, now in progress.

#### IV. DISCUSSION

It may now be fruitful to compare the high-frequency radio-pulse profiles with those obtained at optical wavelengths (Warner *et al.* 1969; Wampler *et al.* 1969; Lynds *et al.* 1968). Optical observations yield the pulse shape shown in Figure 7 (after Warner *et al.* 1969) consisting of a nearly symmetrical main pulse of some 1.5 msec width followed about 13.55 msec later by an interpulse about 3 msec wide with integrated flux density relative to the main pulse (excluding the precursor) and interpulse observed at radiofrequencies seem to correspond to the similar pulses in the optical.

The 0.19-msec discrepancy between radio and optical wavelengths in the interval between the main pulse and the interpulse may be the result of the difference in shape of the corresponding pulses. However, a measurement of the peak-to-peak interval for the optical pulses made by Horowitz (1970) agrees with our 430-MHz value within one sample interval (32  $\mu$ sec). The ratios of the peak flux density and energy of the main pulse to those of the interpulse are similar at radio and optical wavelengths. The pulse widths, however, are very much different in the two regions; at optical wavelengths, the widths are many times the instrumental resolution whereas those at high radiofrequencies may be unresolved. The pulse widths at high radiofrequencies are about an order of magnitude smaller than those observed in the optical. A further obvious difference is the existence of the strongly linearly polarized precursor (Campbell *et al.* 1970) at radiofrequencies. No corresponding feature is observed on the optical pulse.

The relationship of the radio pulse to the optical may be further investigated via a simultaneous observation. Conklin *et al.* (1969) carried out such an observation; however, interpretation of their data depends heavily upon a precise knowledge of the dispersion measure of the pulsar. Using the best dispersion data then available, they showed that the radio and optical pulses were in phase to within 6 msec, the error being largely due to the accuracy with which the dispersion measure was known. The data in Table 3 can now be used to improve upon their preliminary calculations. Using the value for  $D$  from the table, Doppler-corrected to 1969 March 15, the expected group delay between optical frequencies and 424.0 MHz is  $1310.940 \pm 0.03$  msec, which is 39 periods plus  $20.09 \pm 0.03$  msec. The observed delay was 39 periods (assumed) plus  $20.78 \pm 0.28$  msec; that is, the radio pulse arrived later than predicted by about  $0.7 \pm 0.3$  msec.

The question of simultaneity is not really resolved by the previous calculation because it is not clear what feature of the pulse structure was used as a reference by Conklin *et al.* They were not aware of the structure of the main radio pulse (nor did they observe it, as their time resolution was about 3.7 msec) and thus substantially underestimated their experimental error.

The pulse arrival times, measured by Arecibo in the radio region and—not simultaneously—by Harvard in the optical, have also been compared by Horowitz (1970), who accounted for Earth motions and known variations in pulsar period. He reports that the peaks of the optical and 430-MHz main pulses arrive within 200  $\mu$ sec when the radio dispersive delay ( $D/f^2$ ) is removed. Two hundred light- $\mu$ sec is only 60 km, a distance small with respect to the radius of the velocity-of-light circle of the pulsar, and not much larger than the probable dimensions of the neutron star itself. Thus, there can be little doubt of the correspondence of the main and interpulses observed at radio and optical frequencies.

The properties of the radio pulsar in the Crab Nebula have been somewhat clarified by the present radio observations; however, the relation of the radio pulsar to the optical one has also been somewhat complicated. Resolution of the radio main pulse into two components displaying quite dissimilar properties has destroyed any simple correspondence which may once have been assumed to exist between the radio and optical regimes. One must also account for the large pulse widths at optical wavelengths relative to the narrow ones at high radiofrequencies. Indeed, several distinct physical mechanisms operating in the same region or in close proximity seem to be required to account for the various features of the pulsar's radiation.

Further evidence for this point of view is the apparent lack of spectral continuity between the radio and optical regimes. We have discussed above the rather large spectral index which our measurements imply for frequencies above 200 MHz. Two upper limits on the flux density of the pulsar are given in Figure 4. One is by Downs and Reichley (1970) at 2388 MHz, and the other is by one of us (C.C.C.) at 15 GHz (1-GHz bandwidth, 1-msec time constant, and several 10-minute observations). Measurements of the infrared (Neugebauer *et al.* 1969), optical (Oke 1969), and X-ray (Fishman *et al.* 1969)

flux densities from the pulsar yield a spectrum which peaks in the visible and declines fairly steeply at both longer and shorter wavelengths. Thus, the pulsar's spectrum divides into two regimes of emission (optical and radio) separated by several decades of frequency where appreciable emission probably does not occur.

The low-frequency portion of the pulsar's spectrum is well explained in terms of the pulse-broadening model and the high-frequency spectral index as discussed above. However, the high-frequency portion is itself of some interest. Its spectral index is much greater than that of the Crab Nebula ( $-0.3$ ), or even early estimates of the compact source ( $-1.2$ ). If the radio emission were the result of incoherent synchrotron radiation, an electron-energy distribution proportional to  $E^{-7}$  would be implied. Clearly, so precipitous an electron-energy spectrum is incompatible with the optical and X-ray emissions.

The foregoing considerations impose severe constraints on the distribution and motion of charge in the vicinity of the pulsar. A high degree of spatial coherence is seemingly required to account for the radio pulse width and spectral index. Coherence may not be required in the optical regime; our observations are quite consistent with Shklovsky's (1970) explanation in terms of magnetic synchrotron radiation in the presence of a very strong field. Gold (1969*a, b*) and Bertotti, Cavalieri, and Pacini (1969) have proposed a nonmagnetic synchrotron model which invokes a good deal of spatial coherence. Similarly, Caroff and Scargle (1970) have proposed a coherent synchrotron mechanism for the compact source which well may find application in the pulsar itself.

The pulse broadening with wavelength which the pulsar exhibits has been shown to be understandable in terms of a model in which the radio energy of the pulse is scattered in the ionized interstellar medium between the source and the Earth. The pulse smearing at low frequency thus results from the superposition of pulsed flux arriving via many paths of different electrical lengths.

Salpeter (1967, 1969) and Scheuer (1968) have provided a theoretical framework for discussing radio propagation through a region containing random inhomogeneities which is the point of departure for interpretation of interstellar and interplanetary scintillations. The theory does not, however, imply observable scintillation phenomena for NP 0532. Salpeter argues that the pulse broadening is inversely proportional to the frequency interval over which scintillations become decorrelated. Thus, at most radio-frequencies at which the pulsar has been observed, the radiometer bandwidth is usually many times the predicted decorrelation frequency.

Salpeter (1969) has argued that under rather general circumstances, the pulse broadening should scale as  $f^{-4}$ . As discussed above, the frequency dependence of the probability density used to broaden the pulse is compatible with this result independent of the form of the particular function. The uncertainty in  $\delta$  in equation (3) is such, however, that we in no sense verify Salpeter's calculation. Our purpose is only to argue that, given even the approximate validity of Salpeter's  $f^{-4}$  rule, the pulse broadening observed in NP 0532 is compatible with what is known of interstellar scintillations.

The scattering angles required to account for the low-frequency pulse width must be compared with those which have been inferred from the finite angular size of the compact source in the Crab, on the assumption, for example, that the scattering is the result of a screen midway between the Earth and the pulsar. The excess travel time for a ray scattered through an angle  $\theta_{\text{scat}}$  over a direct ray is  $\Delta t = \frac{1}{8}R\theta_{\text{scat}}^2/c$ , where  $R$  is the distance to the source (1.7 kpc) and  $c$  is the velocity of light. The pulse-broadening parameter  $W$  at 81.5 MHz (see Fig. 6) has a value of 0.029 seconds. Equating  $W$  to  $\Delta t$  in order to estimate  $\theta_{\text{scat}}$ , one obtains a value of  $1.1 \times 10^{-6}$  radians. This estimate of  $\theta_{\text{scat}}$  is in quite quite good agreement with Bell and Hewish's (1967) measurement of the diameter of the compact source of  $1. \pm 0.5 \times (10)^{-6}$  radians.

Ever since the discovery of NP 0532 (Staelin and Reifenstein 1968) there has been

speculation about the relationship between the pulsar and the compact source in the Crab. Several good observational arguments now exist to associate the two sources. The extrapolation of the high-frequency pulsar spectrum to lower frequencies is justified by the success of the pulse-broadening model in explaining both the shape of the observed low-frequency pulsar spectrum and the low-frequency pulse shapes.

The earlier discrepancy between the spectra of the pulsar and the compact source has been partially resolved. Bridle's (1970) measurements at 10 and 15 MHz and his correction of the low-frequency data for interstellar absorption lower the spectral index from  $-1.2$  to  $-1.76 \pm 0.15$ . However, the analysis described in the Appendix yields a better estimate for the compact-source spectral index of  $-1.8 (+0.3, -0.5)$  which is more compatible with the pulsar spectral index of  $-2.9 \pm 0.4$ . A better limit at 1407 MHz could only reduce this discrepancy.

As can be seen in Figure 4, an extrapolation of the pulsar's high-frequency spectrum fits the compact source data reasonably well. Also, Erickson *et al.* (1970) have measured both the fluctuating and continuum components of the small-scale structure in the Crab at 121 MHz via VLBI techniques. Their preliminary estimates of flux density are consistent with the data given in Figure 4. At 121 MHz the ratio of pulsed to total power predicted by the pulse-broadening analysis is 0.8, and the sum of both components is 27 flux units.

There are thus three arguments in favor of associating the compact source and the pulsar: the proximity of their positions and very high brightness temperatures which precipitated the speculation, the compatibility of the diverse spectral data for the two sources, and finally the agreement between the scattering-angle estimates obtained from observations of the angular size of the compact source on the one hand and from the pulse broadening on the other. The case for associating the two sources is now greatly enhanced. The identity of the two sources, however, can only be established by experiments which measure both the fluctuating and continuum emissions of the compact source.

The authors would like to thank J. A. Roberts, C. E. Heiles, F. D. Drake, G. H. Pettengill, E. E. Salpeter, G. A. Zeissig, R. F. Jurgens, K. R. Lang, and A. T. Moffet for many valuable discussions, and H. D. A. Cabassa and E. A. Mayo for their programming skill and advice. We are also indebted to A. Parrish for making available his low-frequency receiver system and generous help and to M. A. Feyjoo, F. S. Harris, R. Dugatkin, and their staff for their constant technical support. The authors would also like to thank P. E. Reichley for kindly granting permission to use his unpublished flux upper limit and Paul Horowitz for generously making available his observations relative to the simultaneity of radio and optical emission. One of us (J. M. R.) wishes to acknowledge assistance from NASA grant NGL 16-001-002. Arecibo Observatory is operated by Cornell University under contract with the National Science Foundation with partial support from the Advanced Research Projects Agency. This work was supported in part by the Air Force Office of Scientific Research under contract F44620-69-C-0092. The detection attempt at 15 GHz was made at the Haystack Facility which is operated by MIT Lincoln Laboratory and supported by the U.S. Air Force.

#### APPENDIX

A nonlinear least-squares regression analysis was made to determine the values of  $k$  and  $a$  which minimized the weighted sum of squared residuals,  $\epsilon^2$ ,

$$\epsilon^2 = \sum_{n=1}^N [(O_n - T_n)/\sigma_n]^2, \quad (8)$$

in which  $O_n$  was the observed pulsar flux density in the  $n$ th measurement,  $\sigma_n$  the associated uncertainty (standard deviation), and  $T_n$  the theoretical flux density according to the relation

$$T_n(k, a, f_n) = k(f_n/f_0)^a, \quad (9)$$

in which  $k$  and  $a$  are to be determined and  $f_n$  is the (known) frequency of the  $n$ th measurement. Straight-line ("linear") regression using logarithms was not applied because the error distributions of our pulsar flux measurements were judged to be seriously skewed on a logarithmic scale (see Fig. 4). The large uncertainties, coupled with the nonlinearity of the regression line, also cast serious doubt on the significance of the formal standard deviation of the regression line at low frequencies, even though the goodness of fit, as judged by the residual  $\epsilon^2$ , was reasonable. ( $\epsilon^2 = 0.3$  lies in the fortieth percentile of the  $\chi^2$  distribution with 1 degree of freedom). Confidence limits for the nonlinear curve were derived by plotting contours of  $\epsilon^2$  in the  $(k, a)$ -plane, and by defining the "error envelope" shown in Figure 4 such that flux values outside this envelope correspond to values of  $(k, a)$  having an associated  $\epsilon^2$  greater than 2, i.e., beyond the eighty-fifth percentile.

When a similar analysis is applied to the compact-source data, the results depend strongly on the handling of the 1407-MHz upper limit (Branson 1967). If the 1407-MHz limit is neglected completely, then  $k = 520 \pm 150$  flux units,  $a = 1.6 \pm 0.5$ , and  $f_0 = 40$  MHz, where the confidence limits correspond to  $\epsilon^2$  twice the minimum value of 7.2. The large value of  $\epsilon^2$  implies, however, that the measurements are inconsistent with the fitted curve ( $\chi^2$  with 3 degrees of freedom beyond ninetyth percentile), if the reported standard deviations are taken at face value. If the upper limit of 0.9 flux units is interpreted as a measurement of  $0.6 \pm 0.3$  f.u., then  $k = 14 \pm 9$  f.u.,  $a = -1.8$  ( $-0.5, +0.3$ ) with  $f_0 = 300$  MHz, where the confidence limits again correspond to  $\epsilon^2$  double the minimum value of 11 ( $\epsilon^2 = 11$  corresponds to the ninety-seventh percentile, with 4 degrees of freedom). In this case the large and unsymmetrical error in  $a$  reflects the fact that the error contour is not elliptical but comma-shaped with its tail extending in the direction of more negative  $a$ . Several possibilities suggest themselves. The spectrum of the compact source may be curved in such a direction that applying the same curvature to the pulsar data would bring the data into closer agreement. On the other hand, if the compact-source spectrum is straight, then the small size of the errors should be reexamined.

#### REFERENCES

- Allen, C. W. 1964, *Astrophysical Quantities* (London: Athlone Press).  
 Bell, S. J., and Hewish, A. 1967, *Nature*, **213**, 1214.  
 Bertotti, B., Cavalieri, A., and Pacini, F. 1969, I.A.U. Symposium on X-Ray and  $\gamma$ -Ray Astronomy, Rome.  
 Boldt, E. A., Desai, U. D., Holt, S. S., Serlemitsos, P. J., and Silverburg, R. F. 1969, *Nature*, **223**, 280  
 Branson, N. B. J. A. 1967, *Nature*, **213**, 1211.  
 Bridle, A. H. 1970, *Nature*, **225**, 1035.  
 Campbell, D. B., Heiles, C. E., and Rankin, J. M. 1970, *Nature*, **225**, 527.  
 Caroff, L. J., and Scargle, J. D. 1970, *Nature*, **225**, 168.  
 Cocke, W. J., Disney, M. J., and Taylor, D. J. 1969, *Nature*, **221**, 525.  
 Comella, J. M., Craft, H. D., Jr., Lovelace, R. V. E., Sutton, J. M., and Tyler, G. I. 1969, *Nature*, **221**, 453.  
 Conklin, E. K., Howard, H. T., Miller, J. S., and Wampler, E. J. 1969, *Nature*, **222**, 552.  
 Counselman, C. C., III. 1970, personal communication  
 Craft, H. D., Jr., and Comella, J. M. 1968, *Nature*, **220**, 676.  
 Downs, G. S., and Reichley, P. E. 1970, personal communication.  
 Duthie, J. G., Sturch, C., Richer, H. B., and Rodney, P. 1969, *Science*, **163**, 1320.  
 Erickson, W. C., Knowles, S. H., Kuiper, T. B. H., Broderick, J. J., 1970, personal communication.  
 Fishman, G. J., Harnden, F. R., and Haymes, R. C. 1969, *Ap. J. (Letters)*, **156**, L107.  
 Fritz, G., Henry, R. C., Meekins, J. F., Chubb, T. A., and Friedman, M. 1969, *Science*, **164**, 709.  
 Gardner, F. F., and Davies, R. D. 1966, *Australian J. Phys.*, **19**, 129.  
 Goldstein, S. J., Jr., and Meisel, D. 1969, *Nature*, **224**, 709.  
 Gold, Thomas 1969a, *Nature*, **221**, 25.  
 ———. 1969b, International Symposium on Pulsars and High-Energy Activity in Supernova Remnants, Rome.

- Heiles, C. E., Campbell, D. B., and Rankin, J. M. 1970, *Nature*, **226**, 529.  
Hewish, A., and Okoye, S. E. 1965, *Nature*, **207**, 59.  
Horowitz, Paul. 1970, personal communication.  
Huguenin, G. R., and Taylor, J. H. 1969, *Ap. Letters*, **3**, 107.  
Kellermann, K. I., Pauliny-Toth, I. I. K., and Williams, P. J. S. 1969, *Ap J.*, **157**, 1.  
Lang, K. R. 1969, International Symposium on Pulsars and High-Energy Activity in Supernova Remnants, Rome.  
Lynds, R., Maran, S. P., and Trumbo, D. E. 1969, *Ap. J. (Letters)*, **155**, L121.  
Miller, J. S., and Wampler, E. J. 1969, *Nature*, **221**, 1037.  
Nather, R. E., Warner, B., and MacFarlane, M. 1969, *Nature*, **221**, 527.  
Neugebauer, G., Becklin, E. E., Kristian, J., Leighton, R. B., Snellen, C., and Westphal, J. A. 1969, *Ap. J. (Letters)*, **156**, L115.  
Oke, J. B. 1969, *Ap. J. (Letters)*, **156**, L49.  
Rankin, J. M., Comella, J. M., Craft, H. D., Jr., Richards, D. W., Campbell, D. B., and Counselman, C. C., III 1969, International Symposium on Pulsars and High-Energy Activity in Supernova Remnants, Rome.  
Richards, D. W. 1969, Symposium on the Crab Nebula, Flagstaff, Arizona.  
Richards, D. W., and Comella, J. M. 1969, *Nature*, **222**, 551.  
Richards, D. W., Counselman, C. C., III, Pettengill, G. H., and Rankin, J. M. 1970, *Ap. J. (Letters)*, **160**, L1.  
Salpeter, E. E. 1967, *Ap. J.*, **147**, 433.  
———. 1969, *Nature*, **221**, 31.  
Scheuer, P. A. G. 1968, *Nature*, **218**, 920.  
Shklovsky, I. S. 1970, *Nature*, **225**, 251.  
Staelin, D. H., and Reifenstein, E. C., III. 1968, *Science*, **162**, 1481.  
Staelin, D. H., and Sutton, J. M. 1970, *Nature*, **226**, 69.  
Wampler, E. J., Scargle, J. D., and Miller, J. F. 1969, *Ap. J. (Letters)*, **157**, L1.  
Warner, B., Nather, R. E., and MacFarlane, M. 1969, *Nature*, **222**, 233.  
Whittaker, E., and Robinson, G. 1967, *The Calculus of Observations* (4th ed.; New York: Dover Publications).  
Zeissig, G. A., and Richards, D. W. 1969, *Nature*, **222**, 150.

